Free-Electron Lasers Without Inversion: Design of Two-Magnet Drift Region

A.I. Artemyev[(1,2,3)], Yu.V. Rostovtsev[(2)],
S. Trendafilov[(2)], K. Kapale[(2)],
M.V. Fedorov[(3)], G. Kurizki[(1)],
M.O. Scully[(2)]

[(1)]Department of Chemical Physics, Weizmann Institute of Science, 76100 Rehovot, Israel
[(2)]Department of Physics, Texas A&M University, College Station, Texas, 77843-4242, USA
[(3)]General Physics Institute, 38 Vavilov St., Moscow, 119991, Russia

Abstract

We propose a two-magnet design of a drift region for a free-electron laser without inversion (FELWI). By performing direct calculations of the phase shifts for electrons passing the drift region, we prove that the small-signal gain integrated over the detuning is positive and is inversely proportional to the energy spread of the "hot" electron beam. The dispersion and the geometry of the drift region are specified, and the requirements to the electron beam quality, including the transverse size and the angular spread, are found.

1 Introduction

Free electron lasers (FELs) are able to produce radiation in different domains, from microwaves [1] to X-rays [2]. They have found many applications [3], including nonlinear spectroscopic characterization of quantum wells [4], solid surfaces [5], for near-field surface microscopy [6], infrared photodissociation spectroscopy of molecules [7], laser surgery [8], [9], material research and processing [10], interaction of X-rays with matter [11], etc. The FEL gain is attributed to the interference of the amplified electromagnetic wave E_0 and the waves emitted by the electrons at the wiggler magnets. The phases of the wiggler-induced waves are sensitive to the electron velocity detuning from the resonance. This leads to the odd gain profile shown in Fig. 1. The the constructive interference, which is needed for the positive gain, requires matching these phases and impose limitations on the electron beam energy spread, angular divergence, transverse size, and, consequently on the maximum FEL frequency and power [12].

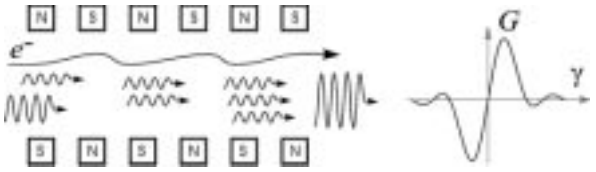

Figure 1. Interference of waves emitted at wiggler magnets and gain of an FEL.

A laser without inversion (LWI) [13] relies on the phase control of the electron transition amplitudes, interference suppression of the stimulated absorption and keeping intact the stimulated emission. This makes the gain possible even if there is no inversion, i.e., if the majority of electrons are in the lower en-

ergy states. The LWI phase control is achieved by the combined action of the external driving laser and the spontaneous relaxation. A new kind of FEL was proposed [14], which implements ideas of lasing without inversion. In an free-electron laser without inversion (FELWI) interfering free-free electron transition amplitudes are formed in wigglers, which are spatially separated by the drift region. The drift region delays different electrons at different phase shifts $\Delta\psi_D$ relative to the amplified wave. For each electron a proper phase delay can lead to a constructive interference of the amplified wave E_0 and the radiation emitted in the two wigglers. Thus the gain profile of an FELWI is positive for all energies, making lasing possible even if there is no inversion, i.e., if there is an equal amount of electrons above and below the resonant energy. The positive small-signal gain profile shown in Fig. 2 makes an FELWI advantageous over an optical klystron or a one-wiggler FEL: for a broad width $\Delta\mathcal{E}$ of the electron energy distribution, an FELWI gain scales as $\sim\ 1/\Delta\mathcal{E}$ and exceeds the gain of a one-wiggler FEL or an optical klystron gain, which scale as $\sim\ 1/\Delta\mathcal{E}^2$. Thus an FELWI can be considered as an optical klystron with an improved phase control or a "phased" optical klystron.

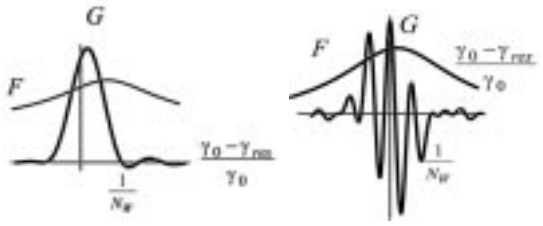

Figure 2. FELWI versus optical klystron gain profile.

The physics of an FELWI was studied in many important details [14]–[19]. It was shown that a FELWI requires a correlation between the transverse electron velocity and the electron energy change in the first wiggler [17]. A non-collinear FEL geometry provides this correlation and allows for the essentially two-dimensional electron dynamics in the drift region, which is needed for the FELWI phase control [17], [18]. It was shown that the FELWI is consistent with the Liouville's and the generalized Madey's theorems [18]. In this sense a multi-dimensional electron dynamics in an FELWI drift region is the classical analog of the spontaneous relaxation in a quantum LWI. Different kinds of drift region phase shifts were studied, including step-like phase shifts [15]–[18] and a linear phase shift [19]. An electron optics design for the linear phase shift was proposed [19].

In this paper, we suggest a two-magnet drift region for an FEL without inversion and prove by direct calculation of electron motion in the drift region that the suggested design indeed gives us FELWI gain. Based on the suggested drift region, we are able to address many important questions of FELWI physics, which remained unsolved: how sensitive is the FELWI phase control to the angular spread of the electron beam, and how much the gain can be enhanced with the phase shifts implemented with the conventional electron optics elements.

The paper is outlined as follows. In Section 2 we describe the electron and field dynamics in the wigglers and find correlations between the electron energy change in the wiggler and their field-induced deflection. In Section 3 we describe the suggested geometry of the drift region and by tracing electron trajectories through the drift region we determine requirements to the electron beam quality and estimate the minimum wavelength of the FEL. In Section 4 we calculate the "hot"-beam gain of the FELWI for an arbitrary linear phase delay in the drift region. We find the acceptable range of the FELWI drift region dispersion and demonstrate how the gain changes with the increasing sensitivity of the drift region phase shift to the field-induced changes of the electron trajectory. Finally, in Section 5 we summarize our results.

2 Electron and field dynamics in a FELWI

The classical electron dynamics in an FEL is described by Hamiltonian

$$H \equiv \gamma mc^2 = \sqrt{(\vec{p} - e\vec{A})^2c^2 + m^2c^4}, \qquad (1)$$

where c is the speed of light, e, m, γ, and $\vec{p}$ are the electron charge, mass, Lorentz factor, and canonical momentum, and

$$\vec{A} \equiv \vec{e}_y A_y = \vec{e}_y (A_L e^{i\psi_L} + A_W e^{i\psi_W} + \ C.C.) \qquad (2)$$

is the vector potential of the combined electromagnetic field of the laser (designated by a subscript L) and the wiggler (designated by a subscript W). The electron and laser beams propagate at the small angles α and θ to the axis of the wiggler, as in Fig. 3. The z-axis is directed along the wiggler, so that $\psi_W = k_W z$, and the phase of the laser field ψ_L equals $k_L(z\cos\theta + x\sin\theta) - \nu_L t + \phi_0$.

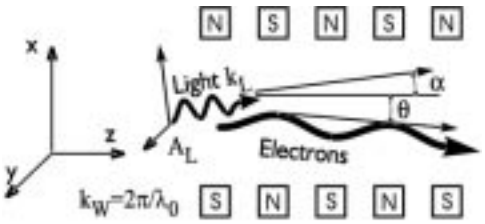

Figure 3. Oblique geometry of an FEL.

The evolution of the slow phase ψ

$$\psi = \psi_L + \psi_W = (\vec{k}_L + \vec{k}_W)\cdot\vec{r} - \nu_L t + \phi_0 \qquad (3)$$

is determined by the pendulum equation, which follows from Eqs. (49)–(53) of the Appendix:

$$\dot{\psi} = \Omega = (\vec{k}_L + \vec{k}_W)\cdot(\vec{\beta} - \vec{\beta}_{res})\, c, \qquad (4)$$

$$\ddot{\psi} \equiv \dot{\Omega} = æ_0 \frac{A_L e^{i\psi} - A_L^* e^{-i\psi}}{i}, \qquad (5)$$

where

$$æ_0 = \frac{2e^2 A_W k_W \nu_L}{m^2\gamma^2 c}, \qquad (6)$$

and $\vec{\beta}_{res} = \vec{v}_{res}/c = \vec{e}_\alpha \nu_L/(c\,\vec{k}_L\cdot\vec{e}_\alpha)$ is the dimensionless resonant electron velocity, $\vec{e}_\alpha = (\sin\alpha, 0, \cos\alpha)$ is the unit vector along the electron beam direction, $\vec{\beta} \equiv \vec{v}/c = \{\beta_x, 0, \beta_z\}$ is the dimensionless electron velocity in the wiggler determined by Eqs. (42)-(45). Initial conditions for Eqs. (4), (5) specify the slow phase $\psi_I(0)$ and $\psi_{II}(T)$ (for the first and second wigglers respectively) and the resonant detuning $\dot{\psi}_I(0) \equiv \Omega_0$ and $\dot{\psi}_{II}(T) \equiv \Omega_1$:

$$\psi_I(0) = \phi_0, \qquad (7)$$

$$\Omega_0 \equiv \dot{\psi}_I(0) = (\vec{k}_L + \vec{k}_W)\cdot\vec{\beta}_0 c - \nu_L, \qquad (8)$$

$$\psi_{II}(T) = \psi_I(T) + \Delta\psi_D, \qquad (9)$$

$$\Omega_1 \equiv \dot{\psi}_{II}(T) = \dot{\psi}_I(T). \qquad (10)$$

We assume in Eqs. (9), (10) that the role of the drift region is to introduce the phase shift $\Delta\psi_D$ and that the resonant detuning Ω is not changed in the drift region: $\dot{\psi}_{II}(T) = \dot{\psi}_I(T)$. The change of the resonant detuning in the drift region can be neglected if we assume that both the electron and laser beams propagate in the second wiggler along its axis. In this case the angular spread $\Delta\alpha_D$ cause negligible, second-order corrections to the initial conditions.

For a non-collinear FEL geometry, $|\alpha| + |\theta| > 0$, the electron dynamics in the first wiggler reveals important correlations. The changes of the resonant detuning $\Delta\Omega_1 = \Omega_I(T) - \Omega_I(0) \equiv \Omega_1 - \Omega_0$ and the slow phase $\Delta\psi_1 = \psi_I(T) - \psi_I(0)$ in the first wiggler correlate with the wiggler-induced changes of the electron energy $\Delta\gamma_1$, the transverse electron velocity $\Delta v_{x\,1}$, the turn angle $\Delta\alpha_1$ of the electron velocity in the first wiggler, and the transverse electron position Δx_1:

$$\begin{aligned} \Delta\gamma_1 &= \frac{\gamma}{2ck_W}\,\Delta\Omega_1, \\ \Delta\alpha_1 = \frac{\Delta v_{x\,1}}{c} &= \frac{\theta-\alpha}{2ck_W}\,\Delta\Omega_1, \\ \Delta x_1 &= \frac{\theta-\alpha}{2k_W}\,\Delta\psi_1. \end{aligned} \qquad (11)$$

We interpret these correlations in terms of the photon emission and absorption: the electrons that absorb energy from the field get deflected in the direction of the laser beam. Depending on their initial conditions, the electrons can earn or loose energy. The angular separation of the "radiating" and "absorbing" electrons makes it possible to treat these electrons differently in the drift region. This provide an additional degree of freedom in the phase control and allows one to arrange the FELWI phase shift.

The pendulum equation (4), (5) is solved by considering the electron-light interaction as a perturbation and expanding the slow phase in the power series over

the laser vector potential, $\psi_I(t) = \psi_I^{(0)}(t) + \psi_I^{(1)}(t)$ in the first wiggler, $0 < t < T$, and $\psi_{II}(t) = \psi_{II}^{(0)}(t) + \psi_{II}^{(1)}(t) + \Delta\psi_D$ in the second wiggler, $T < t < 2T$. The zero-order approximation to the phase ψ is linear in time: $\psi_I^{(0)} = \phi_0 + \Omega_0 t$ and $\psi_{II}^{(0)} = \phi_0 + \Delta\psi_D + \Omega_0 t$ in the first and second wigglers respectively. The first-order corrections $\psi_I^{(1)}$ and $\psi_{II}^{(1)}$ are found by treating the laser field as a perturbation. The iterative procedure is described in [17], [18]. We assume that the laser frequency is close to the resonant frequency ν_{res} determined by the condition $\dot{\psi} = 0$:

$$\nu_{res} = \frac{2ck_W\gamma^2}{1 + K^2/2 + \gamma^2(\alpha - \theta)^2}. \qquad (12)$$

The phase evolution is coupled to the change of the laser field through the Maxwell's equations. The current density $\vec{J} = n_e e\vec{v}$ and the electron velocity $\vec{v}$ are given by Eq. (41) of the Appendix. The wave equation for the laser field envelope A_L is simplified by the slow varying envelope approximation, which allows to neglect second derivatives of the field A_L, and the resonant approximation, which ignores the fast-oscillating terms:

$$\left(\vec{k}_L \cdot \nabla + \frac{\nu_L}{c^2}\frac{\partial}{\partial t}\right) A_L \; = \qquad (13)$$
$$= \left\langle \frac{1}{2i}\,\frac{\mu_0 n_e e^2 (A_L + A_W^* e^{-i(\psi_L + \psi_W)})}{m\gamma} \right\rangle$$
$$\approx \left\langle \frac{N}{i}\, e^{-i\psi} \right\rangle,$$

where angular brackets denote averaging over electron distribution function, $N = \omega_P^2 A_W^*/\nu_L c\gamma$, and $\omega_P^2 = \mu_0 n_e e^2 c^2/m$, and $\mu_0 = 4\pi \cdot 10^{-7}\,\mathrm{N \cdot A^{-2}}$ is permeability of vacuum (SI units). For a stationary FEL operation, $\partial A_L/\partial t$=0, the change of the laser vector potential ΔA_L is found by integrating Eq. (13) over the length of the two wigglers:

$$\Delta A_L \; = \left\langle \int_0^{L_W} \frac{N}{i}\, e^{-i(\psi^{(0)} + \psi^{(1)})}\, dz + \right. \qquad (14)$$
$$\left. + \int_{L_W}^{2L_W} \frac{N}{i}\, e^{-i(\psi^{(0)} + \psi^{(1)} + \Delta\psi_D)}\, dz \right\rangle.$$

For a two-wiggler FEL separated by a drift region, the change of the vector potential ΔA_L of Eq. (14) depends on the initial phase ϕ_0 and the phase shift $\Delta\psi_D$ introduced by drift region. A proper drift region phase shift $\Delta\psi_D$, which can depend on the initial phase ϕ_0, arranges the constructive interference of the amplified radiation and the radiation emitted in the two wigglers by most of electrons regardless of their initial energy. In this papaer, we consider implementation of an FELWI with a linear phase shift

$$\Delta\psi_D = \varsigma + \chi\,\Omega_1\,T \; + \xi\,\Delta\Omega_1\,T \; + \vartheta\,\Delta\psi_1, \qquad (15)$$

where $T = L_W/c$ is the time it takes electrons to pass the wiggler. The coefficients ς, χ, ξ, and ϑ are determined by the drift region geometry. They describe the constant part of the phase shift, the drift region dispersion $T^{-1}\partial\Delta\psi_D/\partial\Omega_1$, and the sensitivity of the phase shift to the change of the resonant detuning $\Delta\Omega_1$ and to the phase change $\Delta\psi_1$ in the first wiggler.

3 FELWI drift region with two magnets

The FELWI phase control can be achieved by making the path length through the drift region sensitive to the electron energy and the transverse electron motion in the wiggler. First, the electron path length should increase at large γ_1 providing the negative dispersion of the drift region, $\partial\Delta\psi_D/\partial\gamma_1 < 0$. This condition is necessary for any FELWI, and we specify the acceptable range of the drift region dispersion below. It was shown [17]–[19] that the this requirement alone is not enough for an FELWI and that the sensitivity of the drift region to the transverse electron motion is essential for the free electron lasing without inversion. In this paper, we explore the phase shift $\Delta\psi_D$ which depends linearly on the direction of the electron velocity after the first wiggler, which is linear in $\Delta\Omega_1$, and and on the wiggler-induced shift of the electron transverse position x_1, which is proportional to the field-induced change of the resonant phase $\Delta\psi_1$ of Eq. (11).

For an FELWI to occur the linearized phase shift,

which also depends on the initial width Δx_0 and angular spread $\Delta\alpha_0$ of the electron beam

$$\begin{aligned}\Delta\psi &= \frac{\partial\Delta\psi_D}{\partial\gamma_1}(\gamma_1-\gamma_{res}) + \\ &\frac{\partial\Delta\psi_D}{\partial\alpha}(\Delta\alpha_0+\Delta\alpha_1) + \\ &\frac{\partial\Delta\psi_D}{\partial x}(\Delta x_0+\Delta x_1) + const,\end{aligned} \tag{16}$$

is to be matched to the linear phase shift of Eq. (15). Note that the initial width Δx_0 and initial angular spread $\Delta\alpha_0$ can wash out the FELWI gain, as they contribute to the "constant" part of the phase shift ς. Thus the FELWI drift region can impose its own limitations on the quality of the electron beam.

The suggested implementations of the FELWI phase shift [17]–[20] assume manipulation of the electron beam with the magnetic optics elements or the optical beam manipulation with the set of prisms or a Bragg reflector. In this paper, for the first time, we suggest and analyze in detail the performance of a magnetic optics set for the FELWI drift region. The set consists of two magnetic lenses which turn the electron beam in the same direction. The sensitivity of angular and coordinate control is achieved by aligning the first magnet almost parallel to the electron beam at the exit from the first wiggler. Then the electrons exiting the first wiggler at slightly different angles meet the first magnet at rather different points and pass the drift region along different routs. The negative dispersion is achieved by letting the high-energy electron, which are less deflected by the first magnet, pass the drift region along a longer route, while lower-energy electrons, which are deflected by the first magnet stronger, pass the drift region along the shorter rout, as shown in Fig. 4.

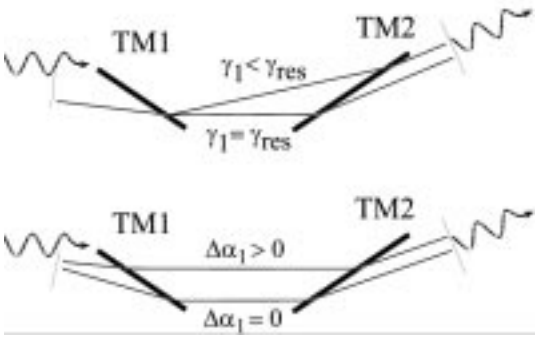

Figure 4. Schema of the phase shift control: negative dispersion and angular and position sensitivity

The suggested drift region design shown in Fig. 5 consists of two magnets. These magnets are assumed to be made of a couple of magnetic plates of different polarity, with the magnetic field directed parallel to the y-axis. The magnet TM1 serves as an electron angular and energy analyzer while the magnet TM2 turns the electron beam further from the original direction, collimates and directs it to the second wiggler.

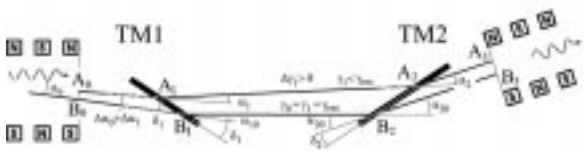

Figure 5. Drift region geometry.

The drift region geometry is characterized by the lengths $B_0B_1 = L_1$, $B_1B_2 = L_2$, $B_2B_3 = L_3$ along the reference trajectory, the angles δ_1, δ_2 between the planes TM1, TM2 and the reference trajectory intervals B_0B_1, B_2B_3 respectively. The magnets deflect the electron at angles α_1 and α_2, which depend on the electron energy and, for the second magnet TM2, on the transverse position B_2A_2:

$$\alpha_1 = \alpha_{10}\left(1-\frac{\gamma_1-\gamma_{res}}{\gamma_{res}}\right), \tag{17}$$

$$\alpha_2 = \alpha_{20}\left(1-\frac{\gamma_1-\gamma_{res}}{\gamma_{res}}-\frac{B_2A_2}{b}\right), \tag{18}$$

where b is the inhomogeneity length for the TM2 magnet. We assume that the deflection angles α_{10} and α_{20} are large as compared to the initial angular spread of the electron beam $\Delta\alpha_0$, its field-induced angular spread $\Delta\alpha_1$, the angles θ and α between the wiggler axis and the propagation directions of the light and electron beams, the angles δ_1 and δ_2 between the TM1 and TM2 magnets and the corresponding intervals B_0B_1 and B_2B_3 of the electron trajectory, and the angular spread $\alpha_1 - \alpha_{10}$ and $\alpha_2 - \alpha_{20}$ introduced by the magnets TM1 and TM2.

We compare different electron trajectories in the drift region with the trajectory of a resonant "reference" electron, which has passed the first wiggler along its axis with the unchanged velocity $\vec{v}_0 = \vec{v}_1 = \vec{v}_{res}$ and energy $\gamma_0 = \gamma_1 = \gamma_{res}$. The trajectory $B_0B_1B_2B_3$ is characterized by its transverse positions B_0, B_1, B_2, B_3 at the exit from the first wiggler W1, at the magnets TM1 and TM2, and at the entrance to the second wiggler W2 respectively.

For an arbitrary electron, which we call "probe", the drift region trajectory $A_0A_1A_2A_3$ is to be found and its length is to be compared to that of $B_0B_1B_2B_3$. In Fig. 5 the "probe" electron was chosen, which increased its energy in the 1-st wiggler and yet entered the drift region at below-resonant energy $\gamma_0 < \gamma_1 < \gamma_{res}$.

The relative phase shift $\Delta\psi_D - \Delta\psi_{D\,ref}$ between the "probe" and the "reference" electrons is determined by the path difference $s_A - s_B \equiv s_{A_0A_1A_2A_3} - s_{B_0B_1B_2B_3}$:

$$\Delta\psi_D - \Delta\psi_{D\,ref} = -\frac{\nu_L}{c}\,(s_A - s_B)\,, \qquad (19)$$

which is found by adding the path differences at the intervals where the "probe" and "reference" electrons move at rather different angles due to the relatively strong deflection α_{10} and α_{20} at the magnets TM1 and TM2: $s_A - s_B \approx (A_1D_1 - C_1B_1) + (D_2A_2 - B_2C_2)$, where $A_1C_1 \perp B_0B_1$, $B_1D_1 \perp A_1A_2$, $B_2D_2 \perp A_1A_2$, and $A_2C_2 \perp B_2B_3$, as shown in Fig. 6.

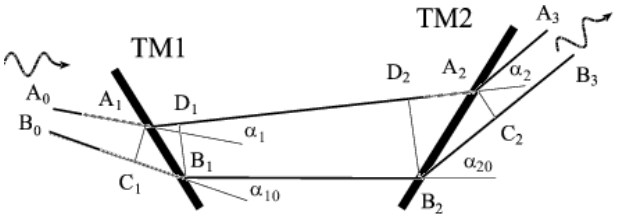

Figure 6. Geometry of the drift region path difference.

It is now straightforward to determine the phase shift $\Delta\psi_D$ of Eq. (19). It is related to that of Eq. (15) by using Eqs. (11), (56), (57) to express the parameters $A_0B_0 = \Delta x_0 + \Delta x_1$, $\Delta\alpha_1$, $\Delta\alpha_0$, $\Delta\gamma_1$, and $\Delta\gamma_0$ through the parameters and variables of the pendulum equation: Ω_0, $\Delta\psi_1$, and $\Delta\Omega_1 = \Omega_1 - \Omega_0$. The linearized phase shift $\Delta\psi_D$ follows:

$$\begin{aligned}\Delta\psi_D \;=\; & \Delta\psi_{D\,ref} \;+ \qquad (20)\\ & +\; \Omega_0 \cdot f_{\Omega_0} \;+\; \Delta\psi_1 \cdot f_{\Delta\psi_1} \;+\; \Delta\Omega_1 \cdot f_{\Delta\Omega_1} \;+\\ & +\; \Delta x_0 \cdot f_{\Delta x_0} \;+\; \Delta\alpha_0 \cdot f_{\Delta\alpha_0},\end{aligned}$$

where the coefficients f_{Ω_0}, $f_{\Delta\Omega_1}$, $f_{\Delta\psi_1}$, $f_{\Delta x_0}$, and $f_{\Delta\alpha_0}$ describe the sensitivity of the phase shift to the initial resonant detuning Ω_0, its wiggler-induced change $\Delta\Omega_1$, the wiggler-induced change of the slow-phase $\Delta\psi_1$, the electron beam width Δx_0 and angular spread $\Delta\alpha_0$. They are described in the Appendix.

The formulas for the phase shift $\Delta\psi_D$ of Eqs. (19), (15) match if

$$f_{\Omega_0} \;=\; \chi\, L_W/c \qquad (21)$$

$$f_{\Delta\Omega_1} \;=\; (\chi + \xi)\, L_W/c \qquad (22)$$

$$f_{\Delta\psi_1} = \vartheta\,. \qquad (23)$$

The drift region dispersion χ and the sensitivity parameters ξ and ϑ of Eq. (15) can be implemented by specifying the drift region geometry: the separation between magnets $L_2 = B_1B_2$, the lengths $L_1 = B_0B_1$ between the wiggler and the first magnet and the orientation angle δ_1 of the first magnet:

$$L_2 \;=\; -\,\chi\, L_W\, \frac{2(1 + K^2/2)}{\alpha_{10}\alpha_{20}\gamma_0^2} \qquad (24)$$

with the optimum dispersion $\chi = -1$,

$$L_1 = L_W \, \frac{\xi + \chi \left(1 - \gamma_0^{-2} (\alpha - \theta)^{-2}\right)}{\vartheta}, \qquad (25)$$

$$\delta_1 = \frac{2\vartheta \, (\theta - \alpha)}{\alpha_{10}(\alpha_{10} + \alpha_{20})} \, \mathcal{K}, \qquad (26)$$

where the factor

$$\mathcal{K} = \left[\frac{1 + K^2/2 + \gamma_0^2 (\alpha - \theta)^2}{\gamma_0^2 (\theta - \alpha)^2} \right] \sim 1$$

can be dropped for $\gamma_0^2 (\theta - \alpha)^2 \gg 1$. The maximum angular spread $\Delta\alpha_0$ and the width Δx_0 of the electron beam are estimated here for the small deflection angles $\alpha_{10},\ \alpha_{20} \ll 1$. The contributions of the angular spread $\Delta\alpha_0$ and the transverse beam width Δx_0 to the phase shift $\Delta\psi_D$ of Eq. (20) should less than one. Thus we estimate the maximum $\Delta\alpha_0$ and Δx_0:

$$\Delta\alpha_0 \leq \frac{1}{k_L L_W} \, \frac{1}{\chi(\theta - \alpha)} \qquad (27)$$

$$\Delta x_0 \leq \frac{1}{k_L} \, \frac{1}{\vartheta \, (\theta - \alpha)} \, \frac{1}{\mathcal{K}}. \qquad (28)$$

The normalized emittance $\varepsilon = \Delta x_0 \, \Delta\alpha_0 \, \gamma_0$ of the electron beam follows:

$$\varepsilon \ \leq \ \frac{1}{\chi\vartheta} \, \frac{1}{k_L^2 L_W} \, \frac{\gamma_0}{(\alpha - \theta)^2} \, \frac{1}{\mathcal{K}}. \qquad (29)$$

The limitation on the minimum FEL wavelength $\lambda_L = 2\pi c/\nu_L$ due to the electron beam emittance follows:

$$\frac{\lambda_L}{2\pi} \geq \sqrt{\frac{L_W \, \varepsilon \, \chi \, \vartheta \, (\alpha - \theta)^2}{\gamma_0} \, \mathcal{K}} \sim \sqrt{\frac{L_W \, \varepsilon \, \chi \, \vartheta}{\gamma_0^3}} \qquad (30)$$

Thus the minimum FELWI wavelength λ_L is related to the electron beam emittannce ε, the drift region dispersion χ and the sensitivity parameter ϑ of Eq. (15).

To reduce the electron beam divergence after the drift region, the inhomogeneity length b is adjusted to collimate the beam. It divergence after the TM2 magnet due to the energy spread, $(\alpha_{10} + \alpha_{20})\Delta\gamma_0/\gamma_0$, is compensated by the focusing term $-\alpha_{20} A_2 B_2/b \sim -\alpha_{20}/b \cdot L_2 \alpha_{10} \Delta\gamma_0/\gamma_0$ of Eq. (18). Thus the TM2 inhomogeneity length b is found:

$$b \ = \ L_2 \frac{\alpha_{10}\alpha_{20}}{\alpha_{10} + \alpha_{10}}. \qquad (31)$$

We summarize the suggested FEL parameters:
Electron beam:
relativistic factor $\gamma_0 = 15$;
velocity angle to the z-axis $\alpha = -0.133\,\mathrm{rad}$;
energy spread $\Delta\gamma_0 = 1$;
emittance $\varepsilon = 40\pi\,\mathrm{mm{\cdot}mrad}$;
angular spread $\Delta\alpha_0 = 5 \cdot 10^{-4}\,\mathrm{rad}$;
transverse size $\Delta x_0 = 4\,\mathrm{mm}$;
Light beam:
wavelength: $\lambda = 359\,\mu\mathrm{m}$;
angle to the z-axis $\theta = 0$;
First wiggler oriented at the angle to the electron and light beams:
period $\lambda_{W1} = 2.73\,\mathrm{cm}$;
number of periods $N_{W1} = 36$;
length $L_{W1} = 0.98\,\mathrm{m}$;
parameter $K = 1.27$;
Second wiggler oriented along the electron and light beams:
period $\lambda_{W2} = 8.79\,\mathrm{cm}$;
number of periods $N_{W2} = 36$;
length $L_{W2} = 3.16\,\mathrm{m}$;
parameter $K = 1.27$;
Drift region:
deflection angle at TM1 $\alpha_{10} = 0.45\,\mathrm{rad}$;
orientation of magnets
$\delta_1 = \delta_2 = 3\alpha_{10}\Delta\gamma_0/\gamma_0 = 0.09\,\mathrm{rad}$;
deflection angle at TM2
$\alpha_{20} = 3\delta_1 = 3\delta_2 = 0.27\,\mathrm{rad}$;
TM2 inhomogeneity length $b = 12.7\,\mathrm{cm}$;
distances between magnets: $L_1 = L_2 = 0.1\,\mathrm{m}$.

The suggested parameters provide the phase shift $\Delta\psi_D$ suitable for free-electron lasing without inversion:

$$\begin{aligned} \Delta\psi_D \ \ = \ \ & const - \Omega_1 T \ + \ 0.6\Delta\Omega_1 T \ - \ 0.07\Delta\psi_1 \\ & - 2 \cdot 10^3 \Delta\alpha_0 + 250\Delta x_0 \end{aligned} \qquad (32)$$

Thus the free-electron lasing without inversion can be achieved in the submillimeter domain with the available electron beams.

4 The FELWI gain

Once the drift region for the FELWI is described, we proceed with the calculations of the gain for the phase shift $\Delta\psi_D$ of Eq. (15). The change of the vector potential of the amplified wave, Eq. (14), is sensitive to the drift region phase shift $\Delta\psi_D$. A particular form of the phase shift

$$\Delta\psi_D^{(0)} = \varsigma + \chi\,\Omega_0\,T = \varsigma + \chi\,\Omega_1\,T - \chi\,\Delta\Omega_1\,T. \quad (33)$$

was analyzed [19] and it was shown that such a phase shift indeed provides an FELWI. In this paper, we extend the results of [19] and find the gain for an arbitrary linear phase shift $\Delta\psi_D$ of Eq. (15). The gain is found by calculating the integrals of Eq. (14) over the lengths of both wigglers. The contribution of the first wiggler is described by the first integral of Eq. (14), which leads to the usual expression for the gain, $G = \Delta|A_L|^2/|A_L|^2$, of a one-wiggler FEL (see [22] and Appendix). The two-wiggler FELWI gain is found by using the perturbation theory approach and considering the $\Delta\psi_D^{(0)}$ part of the phase shift of Eq. (33) as the zero-order approximation to $\Delta\psi_D$ of Eq. (15). The wiggler-induced correction $\Delta\psi_D - \Delta\psi_D^{(0)} = (\xi + \chi)\,\Delta\Omega_1\,T + \vartheta\Delta\psi_1$ is treated as a perturbation. Expanding the right-hand side of Eq. (14) over the first-order terms in the electron-light interaction, we find the change of the laser vector potential A_L and the FELWI gain:

$$G(u) = \frac{e^4 H_W^2 n_e L^3}{2m^3\gamma^3 c^4 \beta_{z\,0}^2 k_W \varepsilon_0} \quad (34)$$
$$\left\langle -\frac{\partial}{\partial u}\,\frac{\sin^2 u\,\cos^2(u + \frac{1}{2}\Delta\psi_D^{(0)})}{u^2} \right.$$
$$+ (\xi + \chi)\frac{\sin^2 u\,\sin(2u + \Delta\psi_D^{(0)})}{u^2}$$
$$\left. -\frac{\vartheta}{4}\,\frac{\partial}{\partial u}\,\frac{\sin^2 u\,\cos(2u + \Delta\psi_D)}{u^2} \right\rangle_{\Delta\psi_D^{(0)} = \varsigma + \chi\,\Omega_0\,T}$$

where $u = \Omega_0 T/2 = (\vec{k}_L + \vec{k}_W)\cdot(\vec{v} - \vec{v}_{res})\,T/2$. The gain of Eq. (34) is expressed as a sum of the three terms. The first term has a form of the total derivative and is similar to the known expression [23] for the optical klystron gain. The other two terms result from the first-order corrections to the drift region phase shift $\Delta\psi_D = \varsigma + \chi\Omega_1 T + \xi\Delta\Omega_1 + \vartheta\Delta\psi_1$. For a negative drift region dispersion, e.g., $\chi = -1$, it is possible to achieve free-electron lasing without inversion by changing the sensitivity parameters ξ or ϑ, as it is shown in Fig. 7. The four curves shown correspond a usual FEL gain profile $G(u)$ for $\xi = 0$ and $\vartheta = 0$ (curve a) and FELWI gain profiles $G(U)$, for increasing sensitivities of the drift region phase shift $\delta\psi_D$ to ξ and ϑ: b) $\xi = 0.5$, $\vartheta = 0$ or $\xi = 0$, $\vartheta = 1$; c) $\xi = 1$, $\vartheta = 0$ or $\xi = 0$, $\vartheta = 2$; d) $\xi = 1.5$, $\vartheta = 0$ or $\xi = 0$, $\vartheta = 3$. For other drift region dispersion $\chi \neq -1$ the sensitivities ξ and ϑ change the shape of the gain profile $G(u)$ differently.

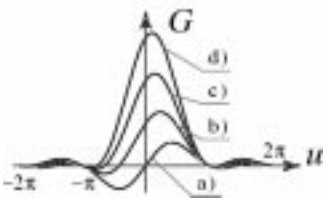

Figure 7. The gain profile $G(u)$ for different sensitivities of the drift region phase shift $\Delta\psi_D$ to the field-induced change of the resonant detuning $\Delta\Omega_1$ and the field-induced change of the slow phase $\Delta\psi_1$. The curves a) — d) are discribed in the text.

To determine the hot-beam gain we average the FELWI gain of Eq. (34) over the broad electron distribution function $f(\gamma)$, such that $\Delta\gamma_0/\gamma_0 \gg 1/N_W = 2\pi/L_W k_W$. The hot-beam FELWI gain $G_{hot} = \int G(u) f(\gamma) du$ follows:

$$G_{hot} = \frac{e^4 H_W^2 n_e L^3 f(\gamma_{res})}{m^3\gamma^3 c^4 \beta_{z\,0}^2 k_W \varepsilon_0}\,\frac{\pi}{4}\,\sin\varsigma \cdot \quad (35)$$
$$\left(\xi \cdot I_\xi \;+\; \vartheta \cdot I_\vartheta\right)$$

where

$$I_\xi = \left(|\chi| + |\chi + 2| - 2|\chi + 1|\right) \quad (36)$$
$$I_\vartheta = -\frac{1}{2}\left(2\,|1 + \chi| - 2\,|2 + \chi| + \chi^2\,\mathrm{sign}[\chi]\right.$$

$$-2\ \mathrm{sign}[1+\chi] - 4\ \chi\ \mathrm{sign}[1+\chi] \qquad (37)$$
$$-2\ \chi^2\ \mathrm{sign}[1+\chi] + 4\ \mathrm{sign}[2+\chi]$$
$$+4\ \chi\ \mathrm{sign}[2+\chi] + \chi^2\ \mathrm{sign}[2+\chi]\Big)$$

The hot-beam FELWI gain G_{hot} of Eq. (35) is proportional to the sensitivity ξ and ϑ of the drift region to the field-induced change of the resonant detuning and the slow phase in the first wiggler. The gain is non-zero only for the negative dispersion $-2 < \chi < 0$ and achieves maximum at $\chi = -1$, as shown in Fig. 8. Thus the combination of the proper negative dispersion and the sensitivity of the phase shift $\Delta\psi_D$ to $\Delta\Omega_1$ and $\Delta\psi_1$ provides lasing without inversion in the two-wiggler system: the gain $G(u)$ is enhanced and its shape changes from an odd to a unipolar profile. For a usual FEL or an optical klystron with positive dispersion, $\chi > 0$, the hot-beam gain turns to zero, because in this case the gain $G(u)$ has positive and negative peaks, which compensate each other. Note that the dependence of the phase shift $\Delta\psi_D$ on the field-induced change of the resonant detuning and phase change in the first wiggler can not be neglected, even though the contribution of these terms, $(\Omega_1 - \Omega_0)T$ and $\psi_1 - \varphi_0$, can be small as compared to $|\Omega_1|T$: without these terms the hot-beam FELWI gain turns to zero according to the Madey's theorem [18], [24].

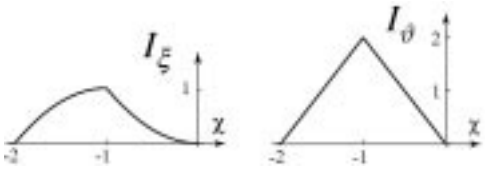

Figure 8. The hot-beam gain of a FELWI determined by the integrals I_ξ and I_ϑ as functions of the drift region dispersion χ.

4.1 Phase distribution in the FELWI

To illustrate the physics of the FELWI operation, we present in Fig. 9 the phase space distribution of the electron beam while it passes the FELWI. Depending on the initial phase ϕ_0, both the electron energy γ and its dimensionless resonant detuning $u = \Omega T$ are increased or decreased, as it is shown in Fig. 9b. The phase shift $\Delta\psi_D$ introduced by the drift region rearranges electrons in the phase space according to their resonant detuning and its change in the first wiggler, Fig. 9b. Then in the second wiggler most electrons loose their energy and contribute to the light amplification. The resulting gain is positive for any resonant detuning, either positive or negative, as it is shown in Fig. 9d. The unipolar gain profile is a characteristic features of a FELWI.

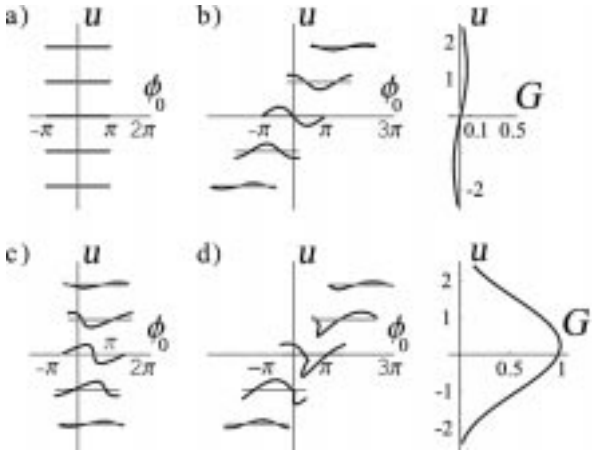

Figure 9. Phase space ditribution of the electron beam at different part of the FELWI:
a) initial distribution;
b) distribution and gain after the first wiggler;
c) distribution after the drift region;
d) distribution and gain after the second wiggler.

5 Conclusions

A realistic design of the drift region, which implements the FELWI gain is suggested and analyzed in detail for the first time. The design simplicity is achieved due to the overall turning of the electron beam in the drift region. The geometry of the drift region is related to the parameters describing the FELWI gain: the drift region dispersion and sensitivity to the field-induced changes of the resonant detuning and phase. The gain profile and the hot-beam gain of an FELWI is found for a linear phase shift of the drift region. It is shown that free-electron

lasing without inversion requires the negative drift region dispersion, which should be limited in the certain range. Another requirement to the phase shift is that the electron path length through the drift region should be sensitive to the direction of the electron velocity or the transverse electron position at the exit from the first wiggler. The minimum FELWI wavelength is found and related to the drift region sensitivity parameters, to the transverse size and angular spread of the electron beam. For available electron beams the suggested FELWI can operate in the submillimeter domain.

The described method for the phase control, which is applied here for an optical klystron, can be adjusted, in principle, for other applications. It can be used for phase corrections and gain enhancement in storage ring FELs because storage rings achieve isochronous motion of the electrons by insertion negative dispersion sections [25], which can serve as a key elements of a drift region for a storage ring FELWI.

6 Acknowledgements

The authors are grateful to L. Narducci, D. Mills, B. Adams, and C. Keitel for illuminating discussions. The authors acknowledge the support from the Office of Naval Research, the National Science Foundation, Texas Engineering Experiment Station, the Robert A. Welch Foundation, and TATP. G.K., M.S., Y.R., and A.I.A. acknowledge the support of the US-Israel BSF, as well as the Russian Foundation for Basic Research grant 02-02-17135 (A.I.A.).

References

[1] H.P. Freund and V.L. Granatstein, Nuclear Instr. & Meth. Phys. Res. A **429**, 33 (1999);

[2] B. Sonntag, Nuclear Instr. & Meth. Phys. Res. A **467 − 468**, 8 (2001);

[3] M.E. Couprie, J.M. Ortega, "Free-electron lasers sources for scientific applications", Analusis **28**, 725-736 (2000);

[4] T. Asano, S. Noda, A. Sasaki, T. Suzuki, T. Mitsuyu, K. Nishi, H. Ohyama, T. Tomimasu, "Ultrafast interband-light modulation by intersubband light (free-electron laser) in quantum wells", Nucl. Inst. & Meth. Phys. Res. B **144**, 123-129 (1998);

[5] G.N. Zhizhin, E.V. Alieva , L. Kuzik, V.A. Yakovlev, D.M. Shkrabo, A.F.G. van der Meer, M.J. van der Wiel, "Free-electron laser for infrared SEW characterization surfaces of conducting and dielectric solids and nm films on them", Appl. Phys. A — Mater. Sc. & Proc **67**, 667-673 (1998);

[6] A. Cricenti, R. Generosi, P. Perfetti, G. Margaritondo, J. Almeida, J.M. Gilligan, N.H. Tolk, C. Coluzza, M. Spajer, D. Courjon, I.D. Aggarwal, "Interface applications of scanning near-field optical microscopy with a free electron laser", Physics Status Solidi A – Applied Research **175**, 317-329 (1999);

[7] M. Putter, G. von Helden, G. Meijer, Chem. Phys. Lett., "Mass selective infrared spectroscopy using a free electron laser" **258**, 118-122 (1996);

[8] J.T. Payne, G.M. Peavy, L. Reinisch, et al., "Cortical bone healing following laser osteotomy using 6.1 mu m wavelength", Laser Surg. Med. **29**, 38-43 (2001);

[9] V.C. Coffey, "Free-electron lasers - Eye surgery application demonstrated with FEL", Laser Focus World **37**, 59-60 (2001);

[10] P.G. O'Shea, H.P. Freund, "Laser technology — Free-electron lasers: Status and Applications", Science **292 (5523)**, 1853-1858 (2001);

[11] S. Doniach, "Fourth-generation X-ray sources: some possible applications to biology", J. Synchrotron Radiat. **7** 116-120, (2000);

[12] S. Reiche, Nuclear Instr. & Meth. Phys. Res. A **445**, 90 (2000);

[13] M.O. Scully, S.Y. Zhu, and A. Gavrielidis, "Degenerate quantum-beat laser: Lasing without inversion and inversion without lasing", Phys. Rev. Lett. **62**, 2813 (1989);

[14] G. Kurizki, M.O. Scully, and C. Keitel, Phys. Rev. Lett. **70**, 1433 (1993);

[15] B.Sherman and G. Kurizki, Phys. Rev. Lett. **75**, 4602 (1995);

[16] D.E. Nikonov, B. Scherman, G. Kurizki, M.O. Scully, Opt. Commun. **123**, 363 (1996);

[17] D.E. Nikonov, M.O. Scully, and G. Kurizki, Phys. Rev. E **54**, 6780 (1996);

[18] D.E. Nikonov, Yu.V. Rostovtsev, and G. Sussmann, Phys. Rev. E **57**, 3444 (1998);

[19] A.I. Artemiev, M.V. Fedorov, Yu.V. Rostovtsev, G. Kurizki, and M.O. Scully, Phys. Rev. Lett. **85**, 4510 (2000);

[20] Y.V. Rostovtsev, G. Kurizki, M.O. Scully, "Broadband optical gain via interference in the free electron laser: Principles and proposed realizations", Phys. Rev. E **64**, 026501 (2001);

[21] Free-Electron Lasers, C. A. Brau, Academic Press, Boston (1990);

[22] F.A. Hopf, P. Meystre, M.O. Scully, W.H. Louisell, Phys. Rev. Lett. **18**, 413 (1976);

[23] G. Datolli, L. Mezi, L. Bucci, Phys. Rev. E **61**, 7052 (2000);

[24] J. M. J. Madey, Nuovo Cimento B **50**, 64 (1978);

[25] M. Giovannozzi, B. Autin, M. Chanel, M. Martini, Ph. Royer, "Application of wigglers to quasi-isochronous transport systems", Proceedings of EPAC 2000, http://accelconf.web.cern.ch/AccelConf /e00/PAPERS/TUP6B09.pdf ; S. Y. Lee, K. Y. Ng, and D. Trbojevic, "Minimizing dispersion in flexible-momentum-compaction lattices", Phys. Rev. E **48**, p. 3040 (1993).

A Equations of motion and gain

The text is splitted into subsections for editing purposes.

A.1 Hamiltonian

The classical electron dynamics in an FEL is described by Hamiltonian

$$H \equiv \gamma mc^2 = \sqrt{(\vec{p} - e\vec{A})^2 c^2 + m^2 c^4} \qquad (38)$$

where c is the speed of light, e, m, γ, and $\vec{p}$ are the electron charge, mass, Lorentz factor, and canonical momentum,

$$\vec{A} \equiv \vec{e}_y A_y = \vec{e}_y (A_L e^{i\psi_L} + A_W e^{i\psi_W} + \ C.C.) \qquad (39)$$

is the vector potential of the combined electromagnetic field of the laser (designated by a subscript L) and the wiggler (designated by a subscript W). The electron and laser beams propagate at the small angles α and θ to the axis of the wiggler, as in Fig. 2. The z-axis is directed along the wiggler, so that $\psi_W = k_W z$, and the phase of the laser field ψ_L equals $k_L(z\cos\theta + x\sin\theta) - \nu_L t + \phi_0$.

A.2 Dynamics along *y*-axis

The Hamiltonian (38) does not depend on y. Therefore the electron canonical momentum in the y-direction is unchanged and is assumed to be zero:

$$\frac{dp_y}{dt} = -\frac{\partial H}{\partial y} = 0, \quad p_y(0) = p_y(t) = 0, \qquad (40)$$

$$\frac{dy}{dt} = \frac{\partial H}{\partial p_y}\bigg|_{p_y=0} = \frac{p_y - eA_y}{\gamma m}\bigg|_{p_y=0} = -\frac{eA_y}{\gamma m} \qquad (41)$$

A.3 Zero-order electron dynamics

The electron interaction with the laser field A_L is treated as a perturbation [21]. In the absence of the laser field the magnetic field of the wiggler $A_y = A_W e^{i\psi_W} + C.C.$ cause oscillations (41) of the electron velocity $\vec{\beta} = \vec{v}/c$ and reduces its projection to the z-axis:

$$\beta_y \equiv \frac{v_y}{c} = -\frac{K\sin(k_W z)}{\gamma}, \qquad (42)$$

$$\frac{dp_x}{dt} = -\frac{\partial H}{\partial x} = 0 \quad p_x = const \qquad (43)$$

$$\beta_x = \frac{\partial H}{c\,\partial p_x} = \frac{p_x}{mc\gamma} = \alpha \quad (44)$$

$$\beta_z = \sqrt{1-\frac{1}{\gamma^2}-\beta_x^2-\beta_y^2} \quad (45)$$

$$= 1-\frac{1+\alpha^2\gamma^2+K^2\,\sin^2(k_W z)}{2\gamma^2}$$

$$\langle\beta_z\rangle = 1-\frac{1+\alpha^2\gamma^2+K^2/2}{2\gamma^2},$$

where angular brackets denote time averaging, and K is the wiggler parameter

$$K=\frac{2eA_W}{mc}=\frac{eH_W}{mck_W}. \quad (46)$$

A.4 First-order electron dynamics

The first-order corrections to the electron canonical momentum $\vec{p}$, energy $mc^2\gamma$, and coordinates x, z are found by the perturbation theory over the electron-light interaction. Eqs. (42)-(45) provide the zero-order approximation and account for the $(A_W e^{i\psi_W} + C.C.)^2$ part of the squared vector potential A_y of Eq. (39). The resonant approximation reduces the remaining part of the squared vector potential $A_y^2 - A_W^2$ to the ponderomotive potential $2(A_L A_W e^{i\psi} + C.C.)$ with the slow phase

$$\psi=\psi_L+\psi_W=(\vec{k}_L+\vec{k}_W)\cdot\vec{r}-\nu_L t+\phi_0. \quad (47)$$

The condition $\dot{\psi}=0$ determines the resonant frequency ν_{res} of the FEL:

$$\nu_{res}=\frac{2ck_W\gamma^2}{1+K^2/2+\gamma^2(\alpha-\theta)^2}. \quad (48)$$

The equations for the electron motion expressed in terms of the slow phase ψ follow:

$$\frac{dp_x}{dt} = \frac{e^2}{\gamma m}2A_W A_L k_L\sin\theta\,\sin\psi \quad (49)$$

$$\frac{dp_z}{dt} = \frac{e^2}{\gamma m}2A_W A_L(k_L\cos\theta+k_W)\,\sin\psi \quad (50)$$

$$\frac{d\gamma}{dt} = \frac{e^2}{\gamma m^2c^2}2A_W A_L\,\nu_L\,\sin\psi. \quad (51)$$

$$\frac{d^2x}{dt^2} = \frac{d}{dt}\left(\frac{p_x}{\gamma m}\right) = \frac{e^2}{m^2\gamma^2}2A_W A_L\cdot \quad (52)$$
$$\cdot\,[k_L\sin\theta-\nu_L/c\cdot\beta_x]\sin\psi$$

$$\frac{d^2z}{dt^2} = \frac{d}{dt}\left(\frac{p_z}{\gamma m}\right) = \frac{e^2}{m^2\gamma^2}2A_W A_L\cdot \quad (53)$$
$$\cdot\,[k_L\cos\theta+k_W-\nu_L/c\cdot\beta_z]\sin\psi,$$

The electron dynamics is governed by the $\sin\psi$ factors in the right-hand sides of Eqs. (49)-(53). Thus it is reduced to the evolution of the slow phase ψ, which is determined by Eqs. (4)–(5) below. This reduction leads to the correlation between the field-induced deflection angle $\Delta\alpha_1$, the changes of the electron energy $\Delta\gamma_1$ and its velocity components Δv_{x1}, Δv_{z1}:

$$\Delta\alpha_1 = \frac{\Delta v_{x1}}{c} = \Delta\gamma_1\,\frac{\theta-\alpha}{\gamma}, \quad (54)$$

$$\Delta v_{x1} = \Delta v_{z1}\,\frac{\theta-\alpha}{\dfrac{1+K^2/2}{\gamma^2}+\alpha(\alpha-\theta)}. \quad (55)$$

We interpret this correlation in terms of the photon emission and absorption in the wiggler: the electrons absorbing photons get the momentum kick towards the light beam.

A.5 Pendulum equation

The evolution of the slow phase ψ of Eq. (47) is determined by the pendulum equation (4), (5), which follows from Eqs. (49)–(53).

A.6 Zero- and first-order approximation to the pendulum equation

The pendulum equation (4)–(8) is solved by considering the electron-light interaction as a perturbation, $\psi_I(t)=\psi_I^{(0)}(t)+\psi_I^{(1)}(t)$ in the first wiggler, $0<t<T$, and $\psi_{II}(t)=\psi_{II}^{(0)}(t)+\psi_{II}^{(1)}(t)+\Delta\psi_D$ in the second wiggler, $T<t<2T$. The zero-order approximation to the phase ψ is linear in time: $\psi_I^{(0)}=\phi_0+\Omega_0 t$ and $\psi_{II}^{(0)}=\phi_0+\Delta\psi_D+\Omega_0 t$ in the first and second wigglers respectively. The first-order corrections $\psi_I^{(1)}$ and $\psi_{II}^{(1)}$ are found by the procedure described in [17], [18].

To relate the pendulum equation in the wiggler with the initial conditions for the electron beam and with the electron dynamics in the drift region, we need to express the initial resonant detuning Ω_0 of Eq. (8) and its change in the first wiggler $\Delta\Omega_1 = \Omega_1 - \Omega_0$ through the electron beam parameters: the initial angular deviation $\Delta\alpha_0$ of the electron velocity from the beam propagation direction α, the initial deviation of the electron relativistic factor γ from the resonance, $\Delta\gamma_0 = \gamma_0 - \gamma_{res}$, and the wiggler-induced change of the relativistic factor $\Delta\gamma_1 = \gamma_1 - \gamma_0$:

$$\begin{aligned}
\Omega_0 &= \Delta\gamma_0 \frac{2ck_W(1+K^2/2)}{\gamma(1+K^2/2+\gamma^2(\alpha-\theta)^2)} \qquad (56)\\
&+ \Delta\alpha_0 \frac{2ck_W\gamma^2(\theta-\alpha)}{\gamma(1+K^2/2+\gamma^2(\alpha-\theta)^2)}\\
&= \Delta\gamma_0 \frac{\nu_L(1+K^2/2)}{\gamma^3} + \Delta\alpha_0\,\nu_L\,(\theta-\alpha)\\
\Delta\Omega_1 &= \Delta\alpha_1 \frac{\nu_L(1+K^2/2+\gamma^2(\alpha-\theta)^2)}{\gamma^2(\theta-\alpha)}\\
&= \Delta\alpha_1 \frac{2ck_W}{\theta-\alpha} \;=\; \Delta\gamma_1 \frac{2ck_W}{\gamma}. \qquad (57)
\end{aligned}$$

A.7 Field evolution - 1

The field evolution in the FELWI is described by Eqs. (13)-(14).

A.8 One-wiggler gain

The contribution of the first wiggler is described by the first integral of Eq. (14), which leads to the usual expression [22] for the gain, $G = \Delta|A_L|^2/|A_L|^2$, of a one-wiggler FEL:

$$G = -\frac{c^2e^4H_W^2\,n_eL_W^3}{8\varepsilon_0\,(mc^2\gamma)^3k_W}\left\langle \frac{d}{du}\,\frac{\sin^2 u}{u^2}\right\rangle_{u=\Omega_0L_W/2c}, \qquad (58)$$

where $\varepsilon_0 = 8.85\cdot 10^{-12}F/m$ is the permittivity of vacuum (SI units), H_W is the amplitude of the magnetic field of the wiggler, L_W is the wiggler length, and n_e is the concentration of electrons. This is a well-known result for the odd gain profile of an FEL: for energies above the resonance most of electrons contribute to the amplification, while for below-resonant energies, most of electrons contribute to the absorption of radiation. For all energies, below or above the resonance, there are electrons contributing to the amplification or absorption of radiation, depending on the phase of the laser field at the moment of the electron entry to the wiggler.

B Drift region geometry

The path differences acquired at each magnet are found from the geometry of the quadrangles $A_1C_1B_1D_1$ and $A_2C_2B_2D_2$ of Fig. 6:

$$\begin{aligned}
A_1D_1 - C_1B_1 &= A_1B_1(\cos(\alpha_{10}+\delta_1) - \cos\delta_1),\\
A_2D_2 - C_2B_2 &= A_2B_2(\cos(\alpha_{20}+\delta_2) - \cos\delta_2). \qquad (59)
\end{aligned}$$

The contributions of other trajectory intervals to the path difference is of the second order of the small angles $\Delta\alpha_0$, $\Delta\alpha_1$, α, θ, δ_1, δ_2, $\alpha_1-\alpha_{10}$, and , $\alpha_2-\alpha_{20}$ and thus can be neglected. The intervals A_1B_1 and A_2B_2 follow:

$$\begin{aligned}
A_1B_1 &= (A_0B_0 + B_0B_1(\Delta\alpha_0+\Delta\alpha_1)\sin\delta_1,\\
A_2B_2 &= B_1B_2\cdot\frac{\alpha_1-\alpha_0+\Delta\alpha_0+\Delta\alpha_1}{\sin(\alpha_{20}+\delta_2)} +\\
&\quad + A_1B_1\cdot\frac{\sin(\delta_1+\alpha_{10})}{\sin(\delta_2+\alpha_{20})} \qquad (60)
\end{aligned}$$

yielding the deviation of the phase shift $\Delta\psi_D$ of the "probe" electron relative to the phase shift $\Delta\psi_{D\,ref}$ of the "reference" electron:

$$\begin{aligned}
&\Delta\psi_D - \Delta\psi_{D\,ref} = \qquad (61)\\
&-\frac{\nu_L}{c}\Big[B_1B_2\big[\big((\alpha_1-\alpha_{10})+(\Delta\alpha_0+\Delta\alpha_1)\big)\cdot\\
&\quad(\cot(\alpha_{20}+\delta_2) - \cos\delta_2\csc(\alpha_{20}+\delta_2))\big] +\\
&+ \big(A_0B_0 + B_0B_1(\Delta\alpha_0+\Delta\alpha_1)\big)\cdot\\
&\quad\big[(\cos(\alpha_{10}+\delta_1)-\cos\delta_1) +\\
&\quad(\cot(\alpha_{20}+\delta_2) - \cos\delta_2\csc(\alpha_{20}+\delta_2))\cdot\\
&\quad\sin(\alpha_{10}+\delta_1)\big]\Big]
\end{aligned}$$

with $\alpha_1 - \alpha_{10}$ and $\alpha_2 - \alpha_{20}$ given by Eqs. (17), (18). The drift region geometry can be chosen so that the linearized phase shift of Eq. (61) coincides with that of Eq. (15). To find the corresponding requirements, the electron position $A_0B_0 = \Delta x_0 + \Delta x_1$ at the exit from the first wiggler, the angular and energy deviations $\Delta\alpha_1$, $\Delta\alpha_0$, $\Delta\gamma_1$, and $\Delta\gamma_0$ are related to the field-induced phase change $\Delta\psi_1$, the initial resonant detuning Ω_0 and its change in the first wiggler $\Delta\Omega_1 = \Omega_1 - \Omega_0$ given by Eqs. (11), (56), (57). The linearized drift region phase shift $\Delta\psi_D$ follows:

$$\begin{aligned}\Delta\psi_D \;=\; & \Delta\psi_{D\,ref} \;+ \\ & +\; \Omega_0 \cdot f_{\Omega_0} \;+\; \Delta\psi_1 \cdot f_{\Delta\psi_1} \;+\; \Delta\Omega_1 \cdot f_{\Delta\Omega_1} \;+ \\ & +\; \Delta x_0 \cdot f_{\Delta x_0} \;+\; \Delta\alpha_0 \cdot f_{\Delta\alpha_0},\end{aligned} \tag{62}$$

where the coefficients f_{Ω_0}, $f_{\Delta\Omega_1}$, $f_{\Delta\psi_1}$, $f_{\Delta x_0}$, and $f_{\Delta\alpha_0}$ describe the sensitivity of the phase shift to the initial resonant detuning Ω_0, its wiggler-induced change $\Delta\Omega_1$, the wiggler-induced change of the slow-phase $\Delta\psi_1$, the electron beam width Δx_0 and angular spread $\Delta\alpha_0$:

$$\begin{aligned} f_{\Omega_0} \;&=\; -\,\frac{\alpha_{10}\tan(\alpha_{20}/2)\gamma_0^2}{c(1+K^2/2)}\,B_1B_2 \\ &\approx\; -\,\frac{\alpha_{10}\alpha_{20}\gamma_0^2}{2c(1+K^2/2)}\,B_1B_2 \end{aligned} \tag{63}$$

$$\begin{aligned} f_{\Delta\psi_1} =\; & \frac{\delta_1\gamma_0^2(\alpha-\theta)(\cos\alpha_{10} - 1 - \sin\alpha_{10}\tan\frac{\alpha_{20}}{2})}{1+K^2/2+(\alpha-\theta)^2\gamma_0^2} \\ & \approx \frac{\delta_1\,\alpha_{10}(\alpha_{10}+\alpha_{20})(\theta-\alpha)}{2(1+K^2/2+(\alpha-\theta)^2\gamma_0^2)} \end{aligned} \tag{64}$$

$$\begin{aligned} f_{\Delta\Omega_1} \;=\; & f_{\Omega_0}\,\frac{1+K^2/2}{1+K^2/2+\gamma^2(\alpha-\theta)^2} \;+ \\ & +\,\frac{\delta_1\gamma_0^2(\alpha-\theta)^2}{c(1+K^2/2+\gamma^2(\alpha-\theta)^2)}\cdot \\ & (\cos\alpha_{10} - 1 - \sin\alpha_{10}\tan\frac{\alpha_{20}}{2})\;B_0B_1 \\ \approx\; & \frac{\gamma_0^2(\theta-\alpha)\delta_1\alpha_{10}(\alpha_{10}+\alpha_{20})}{2c(1+K^2/2+(\alpha-\theta)^2\gamma_0^2)}\,B_0B_1 \\ & -\,\frac{(\alpha_{20}+\delta_2)(\alpha_{10}+\alpha-\theta)}{2c(1+K^2/2+(\alpha-\theta)^2\gamma_0^2)}\,B_1B_2 \end{aligned} \tag{65}$$

$$\begin{aligned} f_{\Delta x_0} \;&=\; \frac{\nu_L}{c}\,\delta_1(\cos\alpha_{10} - 1 - \sin\alpha_{10}\tan\frac{\alpha_{20}}{2}) \\ &\approx\; \frac{\nu_L}{2c}\,\delta_1\alpha_{10}(\alpha_{10}+\alpha_{20}) \end{aligned} \tag{66}$$

$$\begin{aligned} f_{\Delta\alpha_0} \;&=\; \frac{\nu_L}{c}\,\frac{\alpha_{10}(\theta-\alpha)\gamma_0^2\tan\frac{\alpha_{20}^2}{2}}{1+K^2/2}\,B_1B_2 \\ &\approx\; \frac{\nu_L}{c}\,\frac{\alpha_{10}(\theta-\alpha)\gamma_0^2\alpha_{20}^2}{2(1+K^2/2)}\,B_1B_2 \end{aligned} \tag{67}$$

The phase shift of Eq. (62) provides the free-electron lasing without inversion if the coefficients f_{Ω_0}, $f_{\Delta\Omega_1}$, and $f_{\Delta\psi_1}$ ensure the negative dispersion and the sensitivity of the phase shift $\Delta\psi_D$ to the wiggler-induced changes of the resonant detuning and phase of Eq. (15):

$$f_{\Omega_0} \;=\; \chi\,L_W/c \tag{68}$$

$$f_{\Delta\Omega_1} \;=\; (\chi+\xi)\,L_W/c \tag{69}$$

$$f_{\Delta\psi_1} = \vartheta\,. \tag{70}$$

These matching conditions determine the drift region geometry: the lengths L_1 and L_2 and the angle δ_1, which are specified by Eqs. (24)-(26). The condition for compensation of the drift-region induced divergence determines the inhomogeneity length b of the second magnet TM2 (31).